

# Exploring the relationship between the 2D/3D architectural morphology and urban land surface temperature based on a boosted regression tree: A case study of Beijing, China

Zhen Li <sup>a,b</sup>, Dan Hu <sup>a,\*</sup>

<sup>a</sup> State Key Laboratory of Urban and Regional Ecology, Research Center for Eco-Environmental Sciences, Chinese Academy of Sciences, Beijing 100085, China

<sup>b</sup> University of Chinese Academy of Sciences, Beijing 100049, China



## ARTICLE INFO

### Keywords:

Three-dimensional architectural morphology  
Land surface temperature  
Boosted regression trees  
Scale effect  
Landscape metrics

## ABSTRACT

With rapid urbanization, urban three-dimensional morphology and its ecological effects have received more attention. However, thorough investigations into the multiple scale impact of the 2D/3D architectural morphology on urban land surface temperature (LST) remain limited. Taking Beijing as a case study area, we quantified the contributions of the 2D/3D architectural morphology indicators and revealed their marginal effects on multiple scales using the boosted regression trees (BRT) method. The results showed that (1) the building coverage ratio and building height were the most significant factors influencing the LST across all spatial scales and seasons, (2) the 3D shape index, 3D fractal, and 3D adjacency were found to be influential factors, with sum contributions varying from 6.0% to 37.7%, and (3) in summer, the 3D shape index showed a stepwise negative correlation with the LST. The 3D fractal and 3D adjacency exhibited both positive and negative correlations with the LST. When the spatial scale was 240 m, the regulation amplitudes for the 3D shape index, 3D fractal, and 3D adjacency were 2.0°C, 1.0°C and 1.0°C, respectively. These findings provide quantitative insights that can be used to improve urban thermal environments and achieve sustainable urban development by adjusting architectural morphology.

## 1. Introduction

Global urban land area increased by 3.46 million km<sup>2</sup> between 1992–2016 (He et al., 2019), and 55% of the world's population lives in urban areas, with this value increasing continuously (DESA, 2018). Rapid urbanization has altered the urban surface energy balance and has led to urban climate change at regional and local scale (Grimmond, 2007; Kuang et al., 2020; Oke, 2004). The most notable urbanization-induced climate change is the urban heat island (UHI) (Oke, 1973), which refers to higher air temperatures in urban core areas than in surrounding suburban areas. The UHI effect impacts near-surface ecological processes: such as surface energy balance, air quality, precipitation, heatwaves, and building energy consumption (Daramola and Balogun, 2019; Gober et al., 2010; Li et al., 2019; Santamouris et al., 2015; Wan et al., 2012). Meanwhile, UHIs affect urban dweller health and well-being, such as human comfort (Basu and Samet, 2002; Murage et al., 2017). The synergistic effects of rapid urbanization and global warming are likely to aggravate urban thermal conditions in most cities,

which challenges the sustainability of cities (Alavipanah et al., 2017; Sun et al., 2020).

UHI conditions can generally be characterized by air temperature, land surface temperature, and subsurface temperature (Wu et al., 2020). Air temperature captured from conventional meteorological stations has traditionally been used, as these data are highly accurate, have a high temporal resolution and have long-term series. However, a limited number of meteorological stations might cause statistical errors and this remains a great challenge to the study of the spatial heterogeneity of air temperature. Compared to traditional meteorological observation-based approaches, satellite remote sensing technology can provide spatially explicit information across large areas, which is well-suited to studying UHIs (Streutker, 2002).

Numerous studies have shown that the land cover composition and configuration significantly associated with urban LST (Ezimand et al., 2021; Guo et al., 2020; Harmay et al., 2021; Kurniati and Nitivattananon, 2016; Mathew et al., 2017; Peng et al., 2020; Sun et al., 2021; Zhou et al., 2019). Recently, three-dimensional data availability has largely

\* Corresponding author.

E-mail addresses: [lizhen9106@126.com](mailto:lizhen9106@126.com) (Z. Li), [hudan@rcees.ac.cn](mailto:hudan@rcees.ac.cn) (D. Hu).

facilitated three-dimensional urban morphology research, and has led to increasing interest in exploring the relationship between the LST and three-dimensional (3D) urban morphology (Alavipanah et al., 2018; Azhdari et al., 2018; Berger et al., 2017; Hu et al., 2020; Logan et al., 2020; Ren et al., 2020; Sobstyl et al., 2018; Sun et al., 2020). Local climate zones (LCZs), which are categorized by combining land cover and building morphology, are important in the study of the urban climate field (Stewart and Oke, 2012). The LCZ classification system provides standardized climatic observations to describe different local climates in different LCZ categories. 3D building morphology indicators mainly include building height, aspect ratio, building surface fraction, and terrain roughness length. However, the importance of 2D and 3D urban morphology indicators on the LST remains contradictory. For instance, vegetation and impervious surfaces were the most important variables associated with the daytime LST in summer (Hu et al., 2020; Logan et al., 2020). However, other competing studies indicated that 3D urban morphology have a more important role in affecting LST (Chun and Guhathakurta, 2017). Existing studies have mainly focused on the interactive effects of vegetation, buildings, roads, water bodies, and socioeconomic factors (Azhdari et al., 2018; Bokaei et al., 2016; Logan et al., 2020). A comprehensive investigation into the contributions of 2D/3D architectural morphology indicators and marginal effects between LST and 2D/3D architectural morphology indicators at multiple scales remain limited. Marginal effects provide insights into the regulatory role of indicators with a nonlinear relationship and the magnitude in a quantitative way. It is distinguished from previous studies that identified only a positive or negative relationship between the LST and its influencing factors. In addition, there are few 3D architectural morphology indicators available for the LST (Kedron et al., 2019; Liu et al., 2017), especially 3D shape index, 3D fractal and 3D adjacency indicators, which not only properly capture architectural morphological characteristics but are also closely related to the heat transfer process (Yan et al., 2021). For instance, the 3D shape index and 3D fractal, which play important roles in solar radiation, heat absorption and emission, and ventilation, have not yet been considered (Huang and Wang, 2019; Kedron et al., 2019).

This study investigates the impact of 2D/3D architectural morphology indicators on the land surface temperature by adopting a machine learning model (boosted regression trees), and how the impacts vary across spatial scales and seasons. We attempt to address the following two questions: (1) what is the influence and relative contribution of these indicators (3D shape index, 3D fractal, and 3D adjacency) to the LST? and (2) how do 2D/3D architectural morphology indicators that affect LST vary across spatial scales and typical seasons? Addressing these questions can enhance our understanding of the heterogeneity of urban 3D morphology and its relationship with the LST. This investigation can offer insights for urban heat mitigation.

## 2. Methods

### 2.1. Study area

Beijing, the capital of China, covers an area of approximately 16.80 thousand km<sup>2</sup> and supported a total population of 21.51 million in 2018. In addition, 60% of the permanent population residents lived in the inner city, which resulted in excessive population concentration. The climate was a temperate continental monsoon climate characterized by hot, rainy summers and dry, cold winters. The annual mean temperature and annual precipitation were 12.3°C and 600 mm, respectively. Beijing has experienced rapid urban expansion in the vertical and horizontal directions since 1978, and the vertical profile of residential neighborhoods presents a “low-high” pattern from the oldest part of the city to the urban edges (Zheng et al., 2017). Ultrahigh-rise buildings are aggregated in the central business district; for example, the CITIC tower (height: 528 m) is adjacent to the Beijing world towers (height: 350 m). Rapid urbanization and dramatic population growth have changed the

underlying surface, which has led to a series of environmental problems, such as air pollution, and UHIs (Wu et al., 2020). With the Beijing Urban Plan (2016-2035) and Beijing-Tianjin-Hebei Coordinated Development Plan conducted, the Beijing municipal government faced a great challenge between sustainable development and environmental protection. This study focused on Beijing's central city, which covers an area of approximately 660 km<sup>2</sup> (Fig. 1).

### 2.2. Datasets

Building footprints and their floor information were derived from Baidu Maps data circa 2019. By referring to the Pléiades image (part of the study area, which covers an area of 100 km<sup>2</sup>) in 2019 (chromatic sensor with 0.7 m resolution and four multispectral bands with 2.8 m resolution), we found that the locations of the buildings matched well. According to the building design regulations, the building floor average height was set at 3 m. The heights of the buildings were validated by field surveys conducted with a laser rangefinder (Forestry 550, Nikon, JAPAN). The results showed that the actual error was approximately 4.2 m. For the LST retrieval, two cloud-less Landsat-8 OLI images (Spring: May 13, 2019; Summer: July 25, 2019) were acquired from the United States Geological Survey (USGS). To create a homogeneous dataset, 2D/3D architectural morphology indicators and the LST were incorporated into various regular spatial grids using the ArcGIS software (version 10.3).

## 2.3. Methods

### 2.3.1. 2D/3D architectural morphology indicators

Prior studies have adopted numerous metrics to investigate the relationship between urban morphology and the LST using area-based metrics, height-based metrics, volume-based metrics, and composite metrics (Berger et al., 2017; Sun et al., 2020). Here, we incorporated a suite of 2D/3D architectural morphology indicators. Eight indicators were introduced (Table 1). The building coverage ratio, area-weighted mean building height, area-weight mean building height standard deviation, floor area ratio, and building aggregation were the most commonly adopted indicators (Berger et al., 2017; Sun et al., 2020). These indicators interpret the intensity and roughness of the architecture. To our knowledge, the 3D shape index and the 3D fractal were used for the first time to explain the urban LST. The 3D shape index and 3D fractal are comprehensive indices based on the surface area and volume of buildings. Previous studies have proven that the building surface area and volume are influential indicators influencing the LST (Alavipanah et al., 2018; Berger et al., 2017; Hu et al., 2020). Compared to the building surface area and volume, the 3D shape index and 3D fractal adequately capture the heterogeneity, shape complexity, and compactness of architecture (Guerri et al., 2021; Kedron et al., 2019; Qin et al., 2015; Yan et al., 2021). Among the indicators, we developed the 3D adjacency (Fig. 2). The 3D adjacency is a comprehensive index based on the mean distance among adjacent buildings and the height of each building. These indicators interpret the adjacency and compactness. Calculation of the 3D adjacency through the buffer zone, avoids assuming the buildings as the center of mass and then measuring their distance. With this study, we further updated the formulation to serve our purpose. We adopted the methods of Qin et al. 2015 to calculate the 3D fractal.

### 2.3.2. LST retrieval

LST retrieval algorithms from satellite thermal bands can be classified into three categories: the single channel algorithm, multi-channel algorithm (split window algorithm), and multi-angle algorithm (Dwivedi et al., 2018). The single channel algorithm is relatively straightforward and highly accurate. However, the single channel algorithm has higher errors at higher water vapor contents (Jiménez-Muñoz et al., 2014). The split window algorithm performs better than single channel

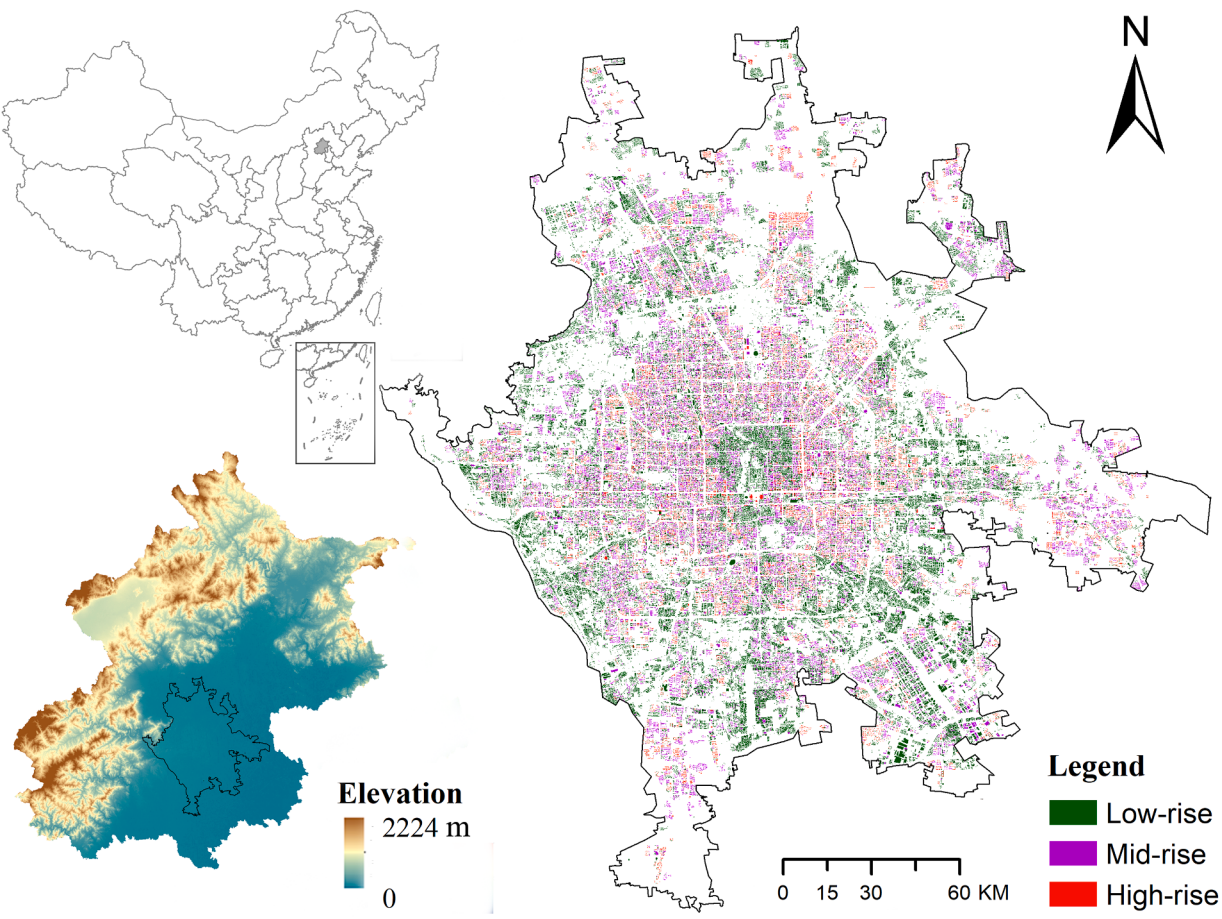


**Fig. 1.** Location of the study area and the distribution of buildings categorized by the number of floors within the study area.

**Table 1**  
2D/3D architectural morphology indicators.

Name	Abbr.	Description	Formulas
Building coverage ratio	BCR	Building coverage ratio of the grid.	$BCR = \frac{\sum_{i=1}^n BS_i}{S_{site}}$
Area-weighted mean building height	BH	The area-weighted average building height.	$BH = \frac{\sum_{i=1}^n BS_i * BH_i}{\sum_{i=1}^n BS_i}$
Mean building height standard deviation	BHstd	Variation degree of the buildings of the grid.	$BHSD = \sqrt{\frac{\sum_{i=1}^n (BH_i - BH)^2}{n}}$
Floor area ratio	FAR	Building area unit area of the grid.	$FAR = \frac{\sum_{i=1}^n c * F}{S_{site}}$
3D shape index	3DSI	The degree of shape complexity.	$3DSI = \frac{\sum_{i=1}^n (BS_i + Li * BH_i)}{3 * v * \sqrt{3v/4\pi}}$
3D fractal	3D fractal	The compactness of the buildings	$\lg N(r) = -D \lg r + c$
Building aggregation	BA	Building aggregation	$BA = \frac{BS_i / S_{site}}{\text{Mean}(D_{building})}$
3D adjacency	3DAD	It measures the adjacency among buildings	$V' = \sum_{i=1}^n S_i * (BH_1 + \dots + BH_n)$ $AD = \frac{V'}{V}$

Notes:  $BS_i$ : building projected area;  $n$ : the number of buildings;  $S_{site}$ : area of the grid.  $BH_i$ : height of building.  $F$ : floor of building.  $c$ : constant.  $Li$ : perimeter of the buildings.  $v$ : volume of buildings of the grid.  $N(r)$ : number of nonempty boxes;  $r$ : scale;  $D$ : 3D fractal dimension.  $D_{building}$ : mean distance between buildings and their nearest neighbor.  $S_i$  is overlapping area of buildings.

algorithm (Jiménez-Muñoz et al., 2014; Rozenstein et al., 2014). A split window algorithm for Landsat 8 bands 10 and 11 was used to determine the LST (Ren et al., 2015). The noise-equivalent change in temperature measured by the thermal infrared sensor (TIRS) (band 10 and band 11) was evaluated using a scene-based method over uniform ground surfaces (including lake, ocean, desert, snow, and dense vegetation) under clear-sky conditions. The noise-equivalent changes in temperature of band 10 and band 11 were 0.05 K and 0.06 K, respectively (Ren et al., 2014). The thermal infrared channel radiance  $B_i(T_i)$  measured at the top of the atmosphere is as follows:

$$B_i(T_i) = \epsilon_i B_i(T_s) \tau_i + (1 - \epsilon_i) R_{atm\_i}^\downarrow \tau_i + R_{atm\_i}^\uparrow$$

where,  $\epsilon_i$  is the effective surface emissivity in channel  $i$ ,  $B_i$  is the Plank function,  $B_i(T_s)$  is the radiance of a black body with surface temperature  $T_s$ ,  $\tau_i$  is the effective transmittance of channel  $i$ ,  $R_{atm\_i}^\downarrow$  and  $R_{atm\_i}^\uparrow$  are the upward and downward atmospheric radiance, respectively, and  $B_i(T_i)$  is the top of atmosphere (TOA) radiance in  $\text{W}/(\text{m}^2 \text{ sr } \mu\text{m})$ .

$$LST = b_0 + \left( b_1 + b_2 \frac{1 - \epsilon}{\epsilon} + b_3 \frac{\Delta \epsilon}{\epsilon^2} \right) + \left( b_4 + b_5 \frac{1 - \epsilon}{\epsilon} + b_6 \frac{\Delta \epsilon}{\epsilon^2} \right) \frac{T_i - T_j}{2} + b_7 (T_i - T_j)^2$$

where,  $T_i$  and  $T_j$  are the brightness temperatures of channel  $i$  and channel  $j$ , respectively.  $\epsilon$  is the average emissivity of channel  $i$  and channel  $j$ ,  $\Delta \epsilon$  is the emissivity of channel  $i$  and channel  $j$ , and  $b_0, \dots, b_7$  is the algorithm coefficient. The coefficients  $b_0, \dots, b_7$  are obtained through numerical analysis.

### 2.3.3. BRT analysis

The boosted regression tree (BRT) method is a powerful approach to

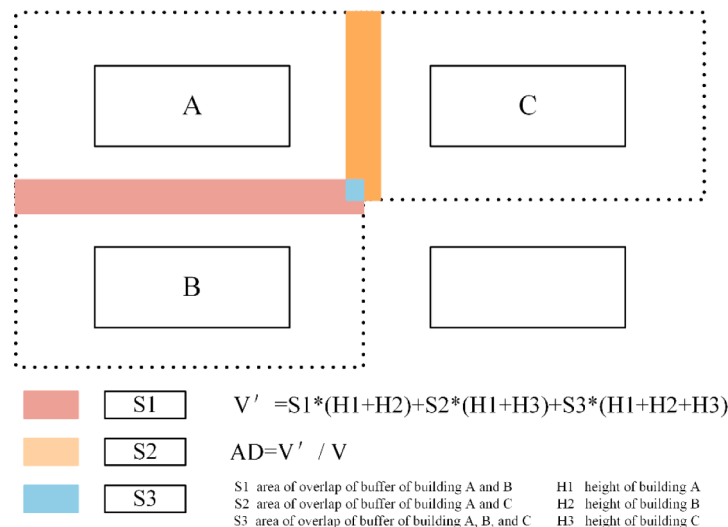


Fig. 2. Calculation of building 3D adjacency.

identify the effect of predictor variables on the LST. Compared to traditional statistical model, a BRT model easily captures complex and nonlinear relationships. For example, the marginal effect of each predictor variable is constant over the whole data space. A BRT uses recursive binary splitting to generate a regression tree algorithm to eliminate the interaction effect among the predictor variables and then uses boosting to build a large ensemble of small regression trees to obtain the nonlinear relationship between the response and its predictor variables. Because of variable splitting, many regression models are estimated across space to avoid possible spatial autocorrelation. A stochastic gradient boosting procedure can improve model performance and reduce overfitting. The BRT method is an iterative process, that adopts the recursive binary segmentation to iteratively fit the tree-based model and to remove the poor trees until a minimum deviation is achieved (Hu et al., 2020). A BRT makes no a priori assumptions regarding the distribution of selected predictor variables or the explanatory variables (Elith et al., 2008). A BRT is robust against collinearity of the predictor variables, interaction effects, non-linear relationships, and spatial autocorrelation of the predictor variables or residuals. Nevertheless, we assessed collinearity among the predictor variables through Pearson's correlation coefficient matrix and variance inflation factor (VIF) tests. When the correlation coefficient between two predictor variables was  $\geq 0.7$ , we removed the predictor variable that correlated with the larger number of variables. Finally, the BA and FAR was removed. Then, we conducted a VIF test, and the results showed that the VIF value of all predictor variables was  $\leq 3.5$ . With the BRTs, the contributions of the selected indicator were determined by the coefficients, which depended on how often the selected indicators were included and the improvement when the selected indicators were selected. The contributions of the selected indicators reached 100%. Partial dependency plots were used to explain the marginal effects of the selected indicators on the LST. The marginal effects show that the potential impacts of the predictor variables vary with changes in their magnitudes. Combining the contributions and marginal effects can assess the importance of the variable impacts. BRT method have gradually received increasing attention in UHI studies (Alavipanah et al., 2018; Hu et al., 2020; Sun et al., 2020). Development of the BRT models was based on dismo package of the R software. The main parameters of the BRT were set to 0.005 (learning rate), 0.5 (bag fraction), 8 (tree complexity), and 10-fold cross validation.

### 3. Results

#### 3.1. Distribution of the 2D/3D architectural morphology indicators and LST

The grid sizes were 60 m, 120 m, 180 m, 240 m, 300 m, and 600 m. The spatial distribution of the 2D/3D architectural indicators (building coverage ratio, building aggregation 3D shape index, and 3D fractal) at 240 m is shown in Fig. 3. The building coverage ratio formed a "high-low-high" pattern from the city center to urban edges (Fig. 3). Likewise, the spatial distributions of the building aggregation and 3D shape were consistent with the building coverage ratio. The city center has the oldest buildings, which have a low-rise profile (height < 10 m) and a high building coverage ratio. The higher building coverage ratio distribution southwest of the study area is attributed to industrial buildings. The spatial distributions of the 3D fractal were concentrated around the Third Ring Road and the Fourth Ring Road with high-rise residential buildings and ultrahigh-rise commercial buildings (Appendix A, supplementary file: Figure 3a). Overall, these indicators showed spatial heterogeneity of architecture and captured the building characteristics in Beijing's central city.

The spatial kernel distribution density of the 2D/3D architectural morphology indicators across all spatial scales is shown in Fig. 4. The building coverage ratio experienced two increases and decreases, and the turning points were approximately 4% and 22%, respectively. The building height was approximately 9 m, with a low degree of variation. The mean building height standard deviation was approximately 2, and the degree of variability decreased with increasing spatial scale. Most of the floor area ratio ranged from 0 to 5 and was centered at 0.1 when the spatial scale exceeded 60 m. The 3D shape index ranged from 1 to 10, and the peak value gradually decreased with increasing spatial scale. The 3D fractal experienced slow growth (when the value of the 3D fractal ranged from 2.00 to 2.30), sharply increased (when the value of the 3D fractal ranged from 2.30 to 2.45), and finally sharply declined (when the value of the 3D fractal ranged from 2.45 to 2.60). The 3D fractal was centered at 2.44. The center of the building aggregation and 3D adjacency gradually increased as the spatial scale increased.

The LST of Beijing's central city at approximately 10:53 am (local time) in spring and summer is shown in Fig. 5. The LST of the study area ranged from  $12.8^{\circ}\text{C}$  to  $59.9^{\circ}\text{C}$  in spring and  $24.8^{\circ}\text{C}$  to  $64.8^{\circ}\text{C}$  in summer. The high LST values were concentrated in places where there was a high building coverage ratio, and the low values were mostly in places where there was high vegetation cover (waterbody).

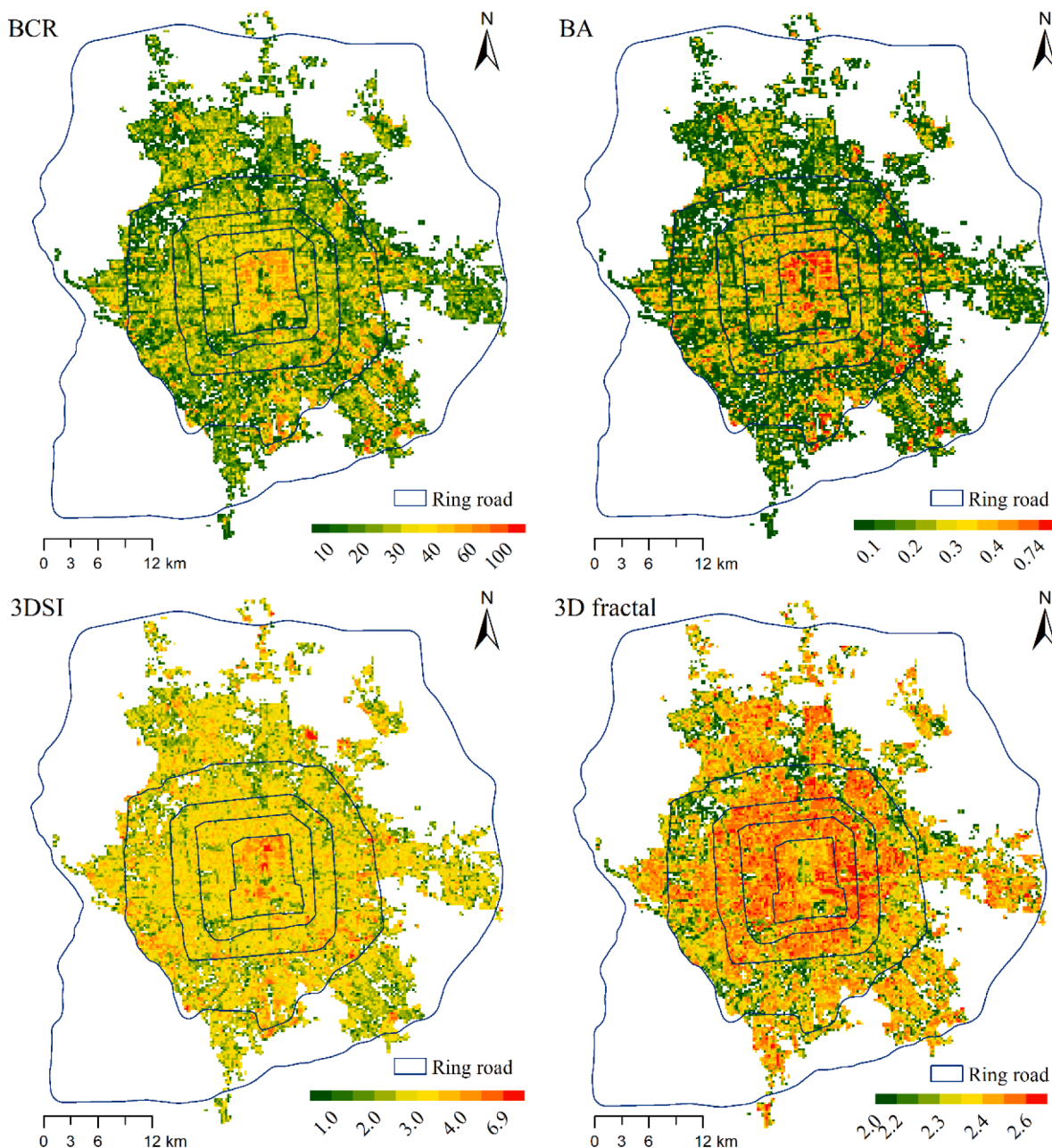


**Fig. 3.** Spatial distribution of the 2D/3D architectural morphology indicators (grid size: 240 m).

### 3.2. Relative contributions

Based on the BRT model, the relative contributions of the 2D/3D architectural morphology indicators to the LST across all spatial scales and seasons are presented in Fig. 6. The dominant indicators influencing the LST were the building coverage ratio and building height. The contributions of the building coverage ratio were largest when the spatial scale was 240 m, at 53.2% and 75.5% in spring and summer, respectively. The contributions of building height became more important when the spatial scales decreased, at 44.3% and 44.9% when the spatial scale was 60 m in spring and summer, respectively. In summer, the sum contributions of the 3D shape index, 3D fractal, and 3D adjacency vary from 37.7% to 6.0% when the spatial scales vary from 600 m to 60 m, respectively.

### 3.3. Marginal effects

The marginal effects of the 2D/3D architectural morphology indicators in summer when the spatial scales were 240 m and 60 m were further analyzed and are shown in Fig. 7. The marginal effect of the 2D/3D architectural morphology indicators on the LST across different spatial scales has similar patterns but differs in magnitude. Generally, the regulation amplitude of specific indicators when the spatial scale was 240 m was larger than that when the spatial scale was 60 m, except for the building height. A high LST most likely occurred in areas with a high building coverage ratio, and low building height. Specifically, the building coverage ratio exhibited a stepwise positive correlation with the LST, and the building height showed a negative correlation with the LST. When the spatial scale was 60 m, the building coverage ratio slowly increased when the building coverage ratio was lower than 20% or exceeded 60% and sharply increased when the building coverage ratio varied from 20% to 60%. When the spatial scale was 60 m, the building

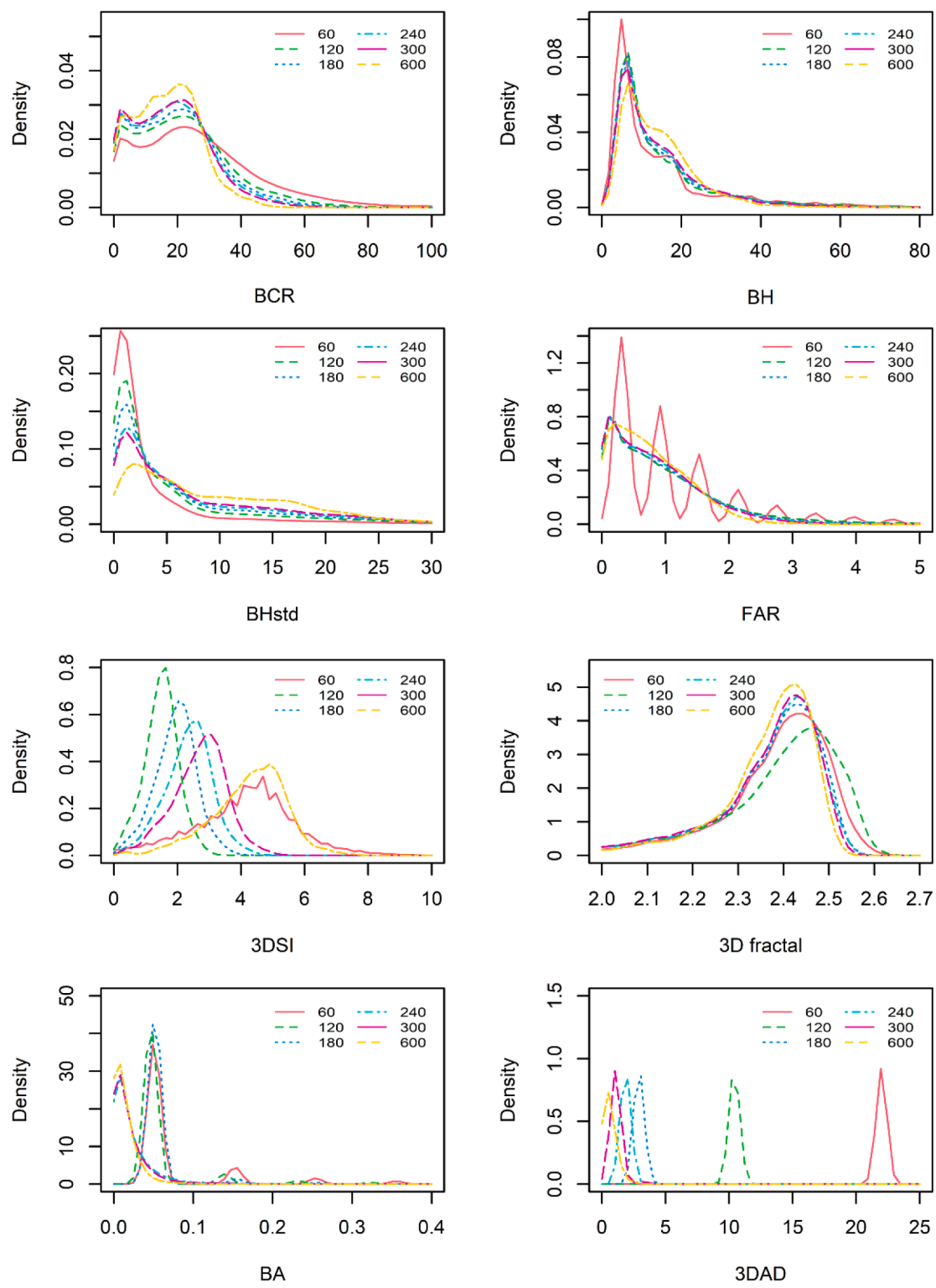


**Fig. 4.** Kernel distribution density of the 2D/3D architectural morphology indicators.

height contribution sharply decreased when the building height was lower than 30 m, slowly decreased when the building height ranged from 30 to 90 m, and then slowed. When the spatial scale was 240 m, the LST regulation amplitudes for the building coverage ratio and building height were  $8.0^{\circ}\text{C}$  and  $2.0^{\circ}\text{C}$ , respectively. When the spatial scale was 60 m, the LST regulation amplitudes for the building coverage ratio and building height were  $4.0^{\circ}\text{C}$  and  $4.0^{\circ}\text{C}$ , respectively.

The 3D adjacency and 3D fractal were complex, combining positive

and negative correlations (the turning points were approximately 1.0 and 2.5 when the spatial scale was 240 m, respectively). When the spatial scale was 240 m, the 3D shape index showed a negative correlation with the LST. A slow decrease in the LST was observed when the 3D shape index ranged from 0 to 4.4, and then a sharp decrease in the LST was observed when the 3D shape index ranged from 4.4 to 4.6, and finally retarded. When the spatial scale was 60 m, the 3D shape index showed a stepwise negative correlation with LST. When the spatial scale

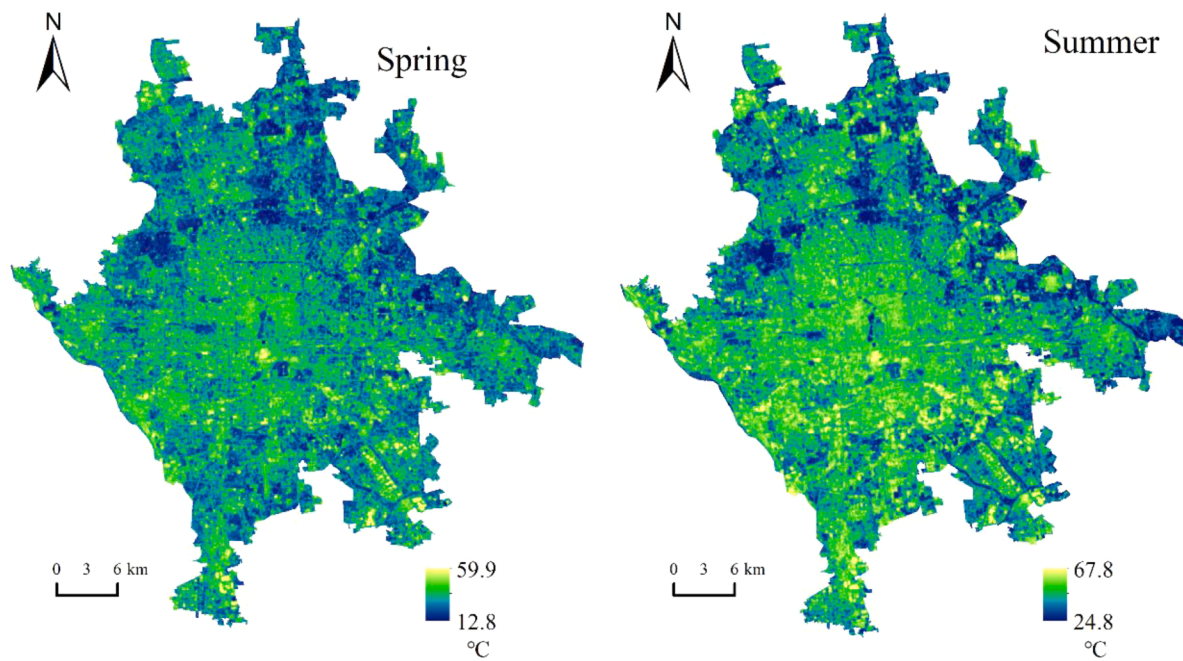


**Fig. 5.** LST derived from Landsat 8 imagery of Beijing's central city.

was 240 m, the LST regulation amplitudes for the 3D adjacency, 3D fractal, and 3D shape index were 1.0°C, 1.0°C and 2.0°C, respectively. When the spatial scale was 60 m, the LST regulation amplitudes for the 3D adjacency, 3D fractal, and 3D shape index were 0.5°C, 2.0°C and 1.0°C, respectively.

#### 4. Discussion

##### 4.1. Effects of 2D/3D architectural morphology indicators on the LST

The architectural morphology affects near-surface energy partitioning and alters the urban thermal environment (Kuang et al., 2020; Yu et al., 2020a). This study focused on the impact of 2D/3D architectural morphology indicators on urban thermal environments across multiple spatial scales and typical seasons in Beijing's central city. Numerous studies have shown that the building coverage ratio and building height had a significant impact on the LST but with different contributions by the same factors to the LST (Guo et al., 2020; Huang and Wang, 2019; Liao et al., 2021; Logan et al., 2020; Mathew et al., 2017; Morabito et al., 2016; Sun et al., 2020; Zheng et al., 2019). Our findings were consistent with previous studies. For instance, the regulation amplitude for the building coverage ratio was 2.7°C in Shanghai, China (Sun et al., 2020). The difference in the regulation amplitude may have resulted from climate, vegetation, image time, and analysis units. The difference in the regulation amplitude for building height may be related to the solar altitude angle and the horizontal distance between the buildings. When vegetation was considered, the relationship between the LST and building height was similar, which indicated that the BRT method was robust (Hu et al., 2020; Sun et al., 2020). The observed discrepancies in the other most influential factors were the result of a suite of indicators. For example, the normalized difference vegetation index (NDVI) was the dominant indicator in summer in the Beijing Olympic Area, with a contribution of 40% (Hu et al., 2020). The role of the 3D shape index was different, which indicated that the surface-based indicator was stronger in explaining the LST than the edge-based indicator (Sun et al., 2020). The relationships between factors and the LST were different due to different mechanisms.

The influence of the building coverage ratio outperformed other architectural morphology indicators for the LST (Fig. 6). The marginal

effect results revealed that increasing the building coverage ratio from 0 to 70% would increase the LST by 8.0°C when the spatial scale was 240 m. These results were consistent with previous studies, but the extent of regulation was different due to distinguishing city characteristics, climate conditions, and analysis units (Sun et al., 2020). Building materials (e.g., concrete and cement) have lower albedos and high solar irradiation absorption (Jamei and Rajagopalan, 2017). Compared to natural land, a higher building coverage ratio increases the sensible heat and reduces the latent heat. A higher building coverage ratio increases the roughness and leads to a low wind speed, thus inducing heat exchange (Huang and Wang, 2019). Regardless, a higher building coverage ratio might release more anthropogenic heat (Stewart and Oke, 2012).

The building height and mean building height standard deviation also played an important role in regulating the LST. The taller the building height is and the larger the mean building height standard deviation of the buildings is, the lower the LST is. These results were consistent with the results of previous studies (Alavipanah et al., 2018; Sun et al., 2020). On the one hand, high-rise buildings improve surface roughness, which leads to turbulence and enhances convective heat dissipation (Berger et al., 2017; Huang and Wang, 2019; Zheng et al., 2019). On the other hand, high-rise buildings cast more shadows, which cause lower temperatures in shaded areas (Dai et al., 2018). A large mean building height standard deviation accelerates air circulation. Our results showed a sharp drop in the LST as the building height increased from 0 to 90 m when the spatial scale was 60 m, and then retarded. Accordingly, high-rise buildings might be beneficial to mitigate the LST.

The 3D shape index and 3D fractal were comprehensive indices based on the building surfaces and building volume, and both were relatively novel 3D architectural morphology indicators that were not included in previous studies. The building volume and surface area were influential indicators of the LST (Alavipanah et al., 2018; Berger et al., 2017; Hu et al., 2020), and large building volumes, surface areas and shape coefficients (ratio between the external surfaces and the volume of the building) caused the LST to rise (Berger et al., 2017; Huang and Wang, 2019; Yu et al., 2020a). A large building surface area means there is more surface to conduct heat. Additionally, large buildings with less compact surface areas might be exposed to solar radiation. Buildings with larger volumes store more heat and generate more anthropogenic

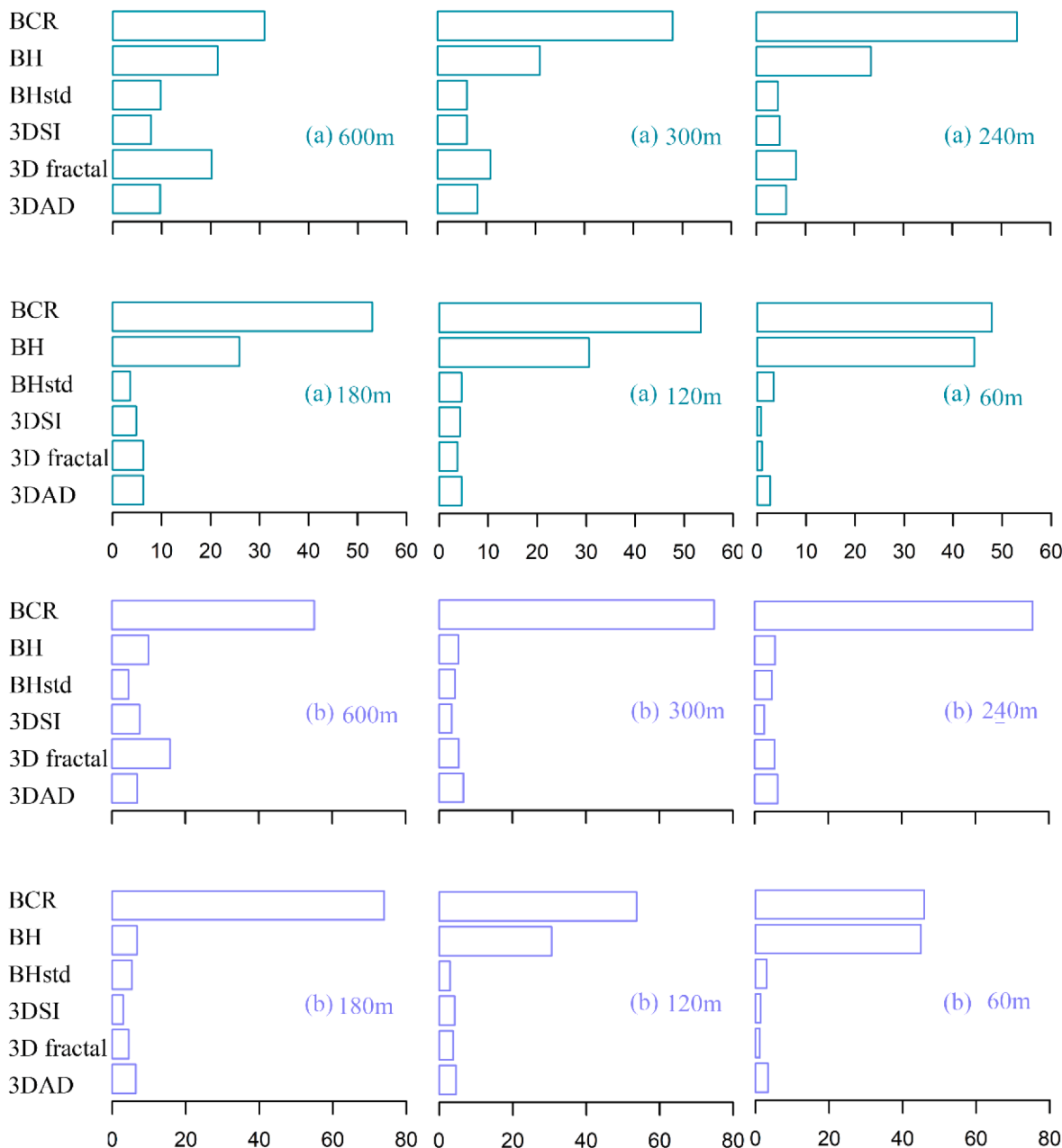


**Fig. 6.** Contributions (%) of the 2D/3D architectural morphology indicators on the LST over different seasons with changes in the spatial scale: (a) spring, and (b) summer, with 60 m, 120 m, 180 m, 240 m, 300 m, 600 m grid sizes.

heat emissions. Previous research has stated that 3D building arrangements have an important impact on air temperature and energy consumption (Alavipanah et al., 2018; Yu et al., 2020b). Our results showed that the relationship between the 3D shape index and the LST was monotonically positive. The 3D fractal showed both positive and negative correlations with the LST. Large building volumes are classified into three scenarios: high building coverage ratio (e.g., low-rise buildings in the city center), high single building projection area (e.g., low-rise industrial sheds in a suburban area), and high building height (e.g., high-rise apartments and commercial buildings around the third road and the fourth road). The proportion of the three scenarios led to a change in the rate of the LST drop, particularly when the spatial scale was 240 m (a turning point was approximately 4.5). Compared to the building volume and surface area, the 3D shape index and 3D fractal adequately capture the heterogeneity of architectural morphology. Additionally, the 3D fractal and 3D shape index can also represent the

indoor space, which reflects the heat exchange capacity between the indoor and outdoor spaces.

The 3D adjacency, which was established based on the distance between adjacent buildings and building height, measures the aggregation and compactness to some extent. The building aggregation was positively correlated with the LST in Berlin but negatively correlated with the air temperature in Beijing (Berger et al., 2017; Tian et al., 2019). The LST increased by 4.4°C when the 3D compactness index increased by 0.1 at a neighborhood scale in a monsoonal humid subtropical climate (Yan et al., 2021). Our results found that the 3D adjacency showed both positive and negative correlations with the LST. A large 3D adjacency can be attributed to an increase in the distance between adjacent buildings or an increase in the height of the buildings. Increasing the distance between adjacent buildings would absorb more solar radiation and enhance ventilation. The coupled effect of increasing the distance between adjacent buildings and increasing the height of the buildings

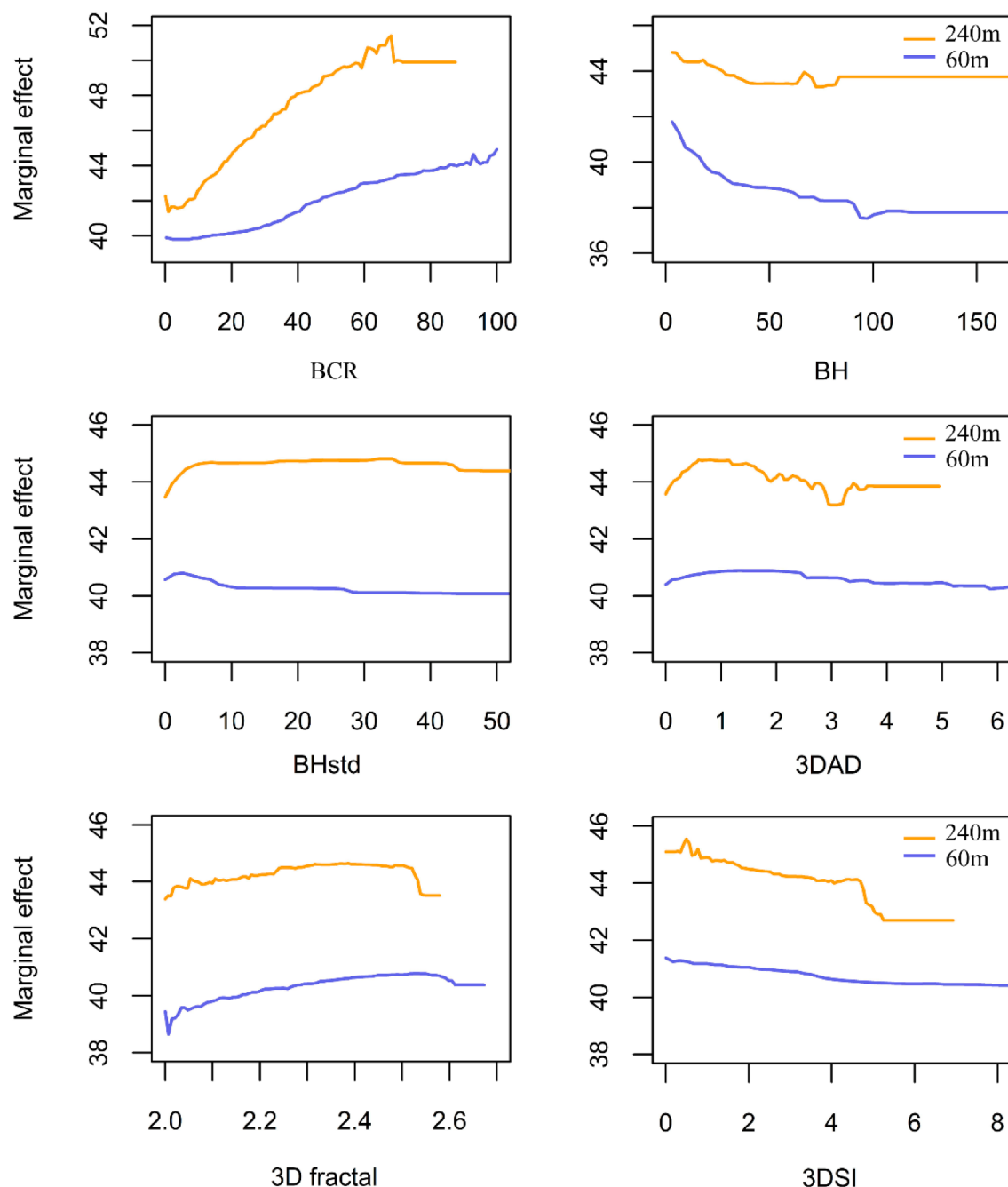


**Fig. 7.** Marginal effects of the most important explanatory variables in summer when the spatial scale was 240 m and 60 m.

led to the 3D adjacency showing both positive and negative correlations with the LST.

#### 4.2. Scale effects of the 2D/3D architectural form indicators on the LST

Exploring the scale effect of the LST and its influencing factors usually applied contrast studies from the view of socioecological hierarchy or changing grids at the community, district, city, and urban agglomeration scales (Peng et al., 2020). Previous studies revealed that the optimal scale for exploring the relationship of the 2D/3D urban morphology and the LST was different in different regions (Lan and Zhan, 2017). For example, the spatial scale, including between 150 m and 540 m (Qiao et al., 2020), 25 m (Yang et al., 2019), 30 m (Alavipanah et al., 2018), 50 m (Hu et al., 2020), 510 m (Gao et al., 2020), and the neighborhood scale (Sun et al., 2020), were adopted to explore the

relationship between the 2D/3D morphology and the LST. Additionally, the suitable spatial scale might be changed when the number of selected metrics changes (Dai et al., 2018). Our study revealed that the association between the 2D/3D architectural morphology indicators and the LST could be scale dependent. On the one hand, some metrics were sensitive to the spatial scales (e.g., 3D shape index). On the other hand, the dominant 2D/3D architectural form indicators influencing the LST changed as the spatial scales changed. The contributions of some indicators became more important as the spatial scale increased (e.g., building height). Appropriate architectural indicators and optical scales need to be considered when studying the LST in the future.

#### 4.3. Architectural morphology planning implications

The results analyzed above can provide guidance to urban planners

on how to develop new districts or redevelop old districts based on the thermal environment. The building coverage ratio and building height should be given more attention. Low-density and high-rise buildings should be built, such as buildings with building coverage ratio approximately 20% and building heights higher than 30 m when the spatial scale is 60 m. Low 3D fractals, 3D adjacency, and 3D shape index were beneficial for mitigating the LST.

#### 4.4. Limitations and future research

Some limitations in our study should be noted. The remotely sensed LST cannot represent the actual surface temperature because it overestimates the horizontal surface temperature and underestimates the vertical surface temperature of features due to the scan angle. Therefore, in situ observations and numerical simulations are vital in acquiring more accurate surface temperatures (Chakraborty et al., 2018; Dewan et al., 2021). The remotely sensed LST was confined, such as low time resolution and clear-sky conditions. Our findings that the relationship between 2D/3D architectural morphology indicators and the LST was statistical relationships. Ecological meteorological processes (e.g., atmospheric and soil processes) were not considered. However, the relationships between different architectural morphology indicators and the LST were different. The mechanisms need to be further researched in the future. However, socioeconomic factors (e.g., human activities and population density), green space, and water bodies are key factors influencing the LST (Dewan et al., 2021; Peng et al., 2018). For instance, socioeconomic factors can explain 12%~20% of UHI intensity variations in major Chinese cities (Li et al., 2020). Green space, electricity consumption and asphalt use are significant factors influencing UHIs in Surabaya city, Indonesia (Kurniati and Nitivattananon, 2016). These factors could be considered to make future work more robust. Additionally, the impact of the background climate, microclimate, albedo, geographies and local climate zones also have an effect on the relationship (Logan et al., 2020). For example, local climate zones have important effects on the surface energy flux and UHI effects (Daramola and Balogun, 2019; Zhao et al., 2014). The role of urban form indicators changed with day/night (Chun and Guhathakurta, 2017; Logan et al., 2020). Regardless, the LST is limited in continuous time, especially at a low temporal resolution, which might ignore microclimate processes. This limitation warrants future study.

Despite these limitations, this study provided quantitative insight into the nonlinear relationship and magnitude between the 2D/3D architectural morphology and LST. In particular, the 3D shape index, 3D fractal, and 3D adjacency can play an important role in mitigating the LST.

#### 5. Conclusion

This study explored the relationship between the 2D/3D architectural morphology indicators and the LST at multiple scales across different seasons in Beijing's central city by adopting BRT method. First, we proposed a suite of 2D/3D architectural morphology indicators. Then, the contributions, marginal effects, and scale effects of the architectural morphology indicators on the LST were derived through the BRT method at different grid sizes. We concluded that the 3D shape index, 3D fractal and 3D adjacency adequately captured the heterogeneity of the architectural morphology. The contributions of the 2D/3D architectural morphology indicators to the LST in spring and summer were similar. The building coverage ratio and building height were the most significant architectural morphology indicators influencing the LST across all spatial scales and seasons. The marginal effects of the building coverage ratio and 3D shape index have different patterns. The marginal effects of building height, 3D adjacency, and 3D fractal have similar patterns across spatial scales but differ in magnitude. The building coverage ratio exhibited a monotonic positive correlation with the LST in summer, with contributions exceeding 45.9% across all

spatial scales. The building height showed a stepwise negative correlation with the LST. When the spatial scale was 240 m, the regulation amplitudes of the building coverage ratio and building height were 8.0°C and 2.0°C, respectively. When the spatial scale was 60 m, the regulation amplitudes of the building coverage ratio and building height were 4.0°C and 4.0°C, respectively. The 3D shape index showed a stepwise negative correlation with the LST. The 3D fractal and 3D adjacency exhibited both positive and negative correlations with the LST. When the spatial scale was 240 m, the LST regulation amplitudes for 3D adjacency, 3D fractal, and 3D shape index were 1.0°C, 1.0°C and 2.0°C, respectively. When the spatial scale was 60 m, the LST regulation amplitudes for 3D adjacency, 3D fractal, and 3D shape index were 0.5°C, 2.0°C and 1.0°C, respectively. Thus, adjusting the architectural compactness, aggregation, and complexity is beneficial to mitigating heat islands.

#### Declaration of Competing Interest

The authors declare that they have no known competing financial interests or personal relationships that could have appeared to influence the work reported in this paper.

#### Acknowledgments

This work was supported by the National Natural Science Foundation of China (No. 41571482 and 42071274).

#### Supplementary materials

Supplementary material associated with this article can be found, in the online version, at doi:[10.1016/j.scs.2021.103392](https://doi.org/10.1016/j.scs.2021.103392).

#### References

- Alavipanah, S., Haase, D., Lakes, T., & Qureshi, S. (2017). Integrating the third dimension into the concept of urban ecosystem services: A review. *Ecological Indicators*, 72, 374–398.
- Alavipanah, S., Schreyer, J., Haase, D., Lakes, T., & Qureshi, S. (2018). The effect of multi-dimensional indicators on urban thermal conditions. *Journal of Cleaner Production*, 177, 115–123.
- Azhdari, A., Soltani, A., & Alidadi, M. (2018). Urban morphology and landscape structure effect on land surface temperature: Evidence from Shiraz, a semi-arid city. *Sustainable Cities and Society*, 41, 853–864.
- Basu, R., & Samet, J.M. (2002). Relation between elevated ambient temperature and mortality: A review of the epidemiologic evidence. *Epidemiologic Reviews*, 24, 190–202.
- Berger, C., Rosentreter, J., Voltersen, M., Baumgart, C., Schmullius, C., & Hese, S. (2017). Spatio-temporal analysis of the relationship between 2D/3D urban site characteristics and land surface temperature. *Remote Sensing of Environment*, 193, 225–243.
- Bokaei, M., Zarkesh, MK., Arasteh, PD., & Hosseini, A. (2016). Assessment of Urban Heat Island based on the relationship between land surface temperature and Land Use/Land Cover in Tehran. *Sustainable Cities and Society*, 23, 94–104.
- Chun, B., & Guhathakurta, S. (2017). Daytime and nighttime urban heat islands statistical models for Atlanta. *Environment and Planning B-Urban Analytics and City. Science*, 44, 308–327.
- Dai, Z., Guldmann, J-M., & Hu, Y. (2018). Spatial regression models of park and land-use impacts on the urban heat island in central Beijing. *Science of the Total Environment*, 626, 1136–1147.
- Daramola, MT., & Balogun, IA. (2019). Local climate zone classification of surface energy flux distribution within an urban area of a hot-humid tropical city. *Urban Climate*, 29.
- Dewan, A., Kiselev, G., Drlik, B., Mahmud, G., et al. (2021). Surface urban heat island intensity in five major cities of Bangladesh: patterns, drivers and trends. *Sustainable Cities and Society*, 71, Article 102926.
- DESA, U (2018). *World Urbanisation Prospects, 2018 Revision*. Retrieved from New York.
- Elith, J., Leathwick, JR., & Hastie, T. (2008). A working guide to boosted regression trees. *Journal of Animal Ecology*, 77, 802–813.
- Ezimand, K., Chahardoli, M., Azadbakht, M., & Matkan, AA. (2021). Spatiotemporal analysis of land surface temperature using multi-temporal and multi-sensor image fusion techniques. *Sustainable Cities and Society*, 64.
- Gao, S., Zhan, Q., Yang, C., & Liu, H. (2020). The Diversified Impacts of Urban Morphology on Land Surface Temperature among Urban Functional Zones. *International Journal of Environmental Research and Public Health*, 17.
- Gober, P., Brazel, A., Quay, R., Myint, S., Grossman-Clarke, S., Miller, A., et al. (2010). Using Watered Landscapes to Manipulate Urban Heat Island Effects: How Much Water Will It Take to Cool Phoenix? *Journal of the American Planning Association*, 76, 109–121.

- Grimmond, S. (2007). Urbanization and global environmental change: local effects of urban warming. *Geographical Journal*, 173, 83–88.
- Guerrri, G., Crisci, A., Messeri, A., Congedo, L., Munafò, M., & Morabito, M. (2021). Thermal Summer Diurnal Hot-Spot Analysis: The Role of Local Urban Features Layers. *Remote Sensing*, 13.
- Guo, A., Yang, J., Sun, W., Xiao, X., Cecilia, JX., Jin, C., et al. (2020). Impact of urban morphology and landscape characteristics on spatiotemporal heterogeneity of land surface temperature. *Sustainable Cities and Society*, 63.
- Harmay, NSM., Kim, D., & Choi, M. (2021). Urban Heat Island associated with Land Use/Land Cover and climate variations in Melbourne. *Australia. Sustainable Cities and Society*, 69.
- He, C., Liu, Z., Gou, S., Zhang, Q., Zhang, J., & Xu, L. (2019). Detecting global urban expansion over the last three decades using a fully convolutional network. *Environmental Research Letters*, 14.
- Hu, Y., Dai, Z., & Guldmann, J-M. (2020). Modeling the impact of 2D/3D urban indicators on the urban heat island over different seasons: A boosted regression tree approach. *Journal of Environmental Management*, 266.
- Huang, X., & Wang, Y. (2019). Investigating the effects of 3D urban morphology on the surface urban heat island effect in urban functional zones by using high-resolution remote sensing data: A case study of Wuhan, Central China. *Isprs Journal of Photogrammetry and Remote Sensing*, 152, 119–131.
- Jamei, E., & Rajagopalan, P. (2017). Urban development and pedestrian thermal comfort in Melbourne. *Solar Energy*, 144, 681–698.
- Jiménez-Muñoz, JC., Sobrino, JA., Skokovic, D., Mattar, C., & Cristobal, J. (2014). Land surface temperature retrieval methods from Landsat-8 thermal infrared sensor data. In , 11. *IEEE Geoscience Remote Sensing Letter* (pp. 1840–1843).
- Kedron, P., Zhao, Y., & Frazier, AE. (2019). Three dimensional (3D) spatial metrics for objects. *Landscape Ecology*, 34, 2123–2132.
- Kuang, W., Li, Z., & Hamdi, R. (2020). Comparison of surface radiation and turbulent heat fluxes in Olympic Forest Park and on a building roof in Beijing. *China. Urban Climate*, 31.
- Kurniati, AC., & Nitivattananon, V. (2016). Factors influencing urban heat island in Surabaya. *Indonesia. Sustainable Cities and Society*, 27, 99–105.
- Lan, Y., & Zhan, Q. (2017). How do urban buildings impact summer air temperature? The effects of building configurations in space and time. *Building and Environment*, 125, 88–98.
- Li, Y., Zhang, J., Sailor, DJ., & Ban-Weiss, GA. (2019). Effects of urbanization on regional meteorology and air quality in Southern California. *Atmospheric Chemistry and Physics*, 19, 4439–4457.
- Li, Y., Sun, YW., Li, JL., & Cao, C. (2020). Socioeconomic drivers of urban heat island effect: empirical evidence from major Chinese cities. *Total of the Environment*, 63, Article 102425.
- Liao, W., Hong, T., & Heo, Y. (2021). The effect of spatial heterogeneity in urban morphology on surface urban heat islands. *Energy & Buildings*, 244, Article 111027.
- Liu, M., Hu, YM., & Li, CL. (2017). Landscape metrics for three-dimensional urban building pattern recognition. *Applied Geography*, 87, 66–72.
- Logan, TM., Zaitchik, B., Guikema, S., & Nisbet, A. (2020). Night and day: The influence and relative importance of urban characteristics on remotely sensed land surface temperature. *Remote Sensing of Environment*, 247.
- Mathew, A., Khandelwal, S., & Kaul, N. (2017). Investigating spatial and seasonal variations of urban heat island effect over Jaipur city and its relationship with vegetation, urbanization and elevation parameters. *Sustainable Cities and Society*, 35, 157–177.
- Morabito, M., Crisci, A., Messeri, A., et al. (2016). The impact of built-up surfaces on land surface temperatures in Italian urban areas. *Total of the Environment*, 551, 317–326.
- Murage, P., Hajat, S., & Kovats, RS. (2017). Effect of night-time temperatures on cause and age-specific mortality in London. *Environmental Epidemiology*, 1, 1.
- Oke, TR. (1973). CITY SIZE AND URBAN HEAT ISLAND. *Atmospheric Environment*, 7, 769–779.
- Oke, TR (2004). Initial guidance to obtain representative meteorological observations at urban sites. *University of British Columbia, Vancouver*.
- Peng, J., Jia, J., Liu, Y., Li, H., & Wu, J. (2018). Seasonal contrast of the dominant factors for spatial distribution of land surface temperature in urban areas. *Remote Sensing of Environment*, 215, 255–267.
- Peng, J., Qiao, R., Liu, Y., Blaschke, T., Li, S., Wu, J., et al. (2020). A wavelet coherence approach to prioritizing influencing factors of land surface temperature and associated research scales. *Remote Sensing of Environment*, 246.
- Qiao, Z., Han, X., Wu, C., Liu, L., Xu, X., Sun, Z., et al. (2020). Scale Effects of the Relationships between 3D Building Morphology and Urban Heat Island: A Case Study of Provincial Capital Cities of Mainland China. *Complexity*, 2020.
- Qin, J., Fang, C., Wang, Y., Li, G., & Wang, S. (2015). Evaluation of three-dimensional urban expansion: A case study of Yangzhou City, Jiangsu Province, China. *Chinese Geographical Science*, 25, 224–236.
- Ren, C., Cai, M., Li, X., Shi, Y., & See, L. (2020). Developing a rapid method for 3-dimensional urban morphology extraction using open-source data. *Sustainable Cities and Society*, 53.
- Rosenstein, O., Qin, Z., Derimian, Y., & Karnieli, A. (2014). Derivation of land surface temperature for Landsat-8 TIRS using a split window algorithm. *Sensors*, 14, 5768–5780.
- Ren, H., Du, C., Liu, R., Qin, Q., Meng, J., Li, Z-L., et al. (2014). Evaluation of Radiometric Performance for the Thermal Infrared Sensor Onboard Landsat 8. *Remote Sensing*, 6, 12776–12788.
- Ren, H., Du, C., Liu, R., Qin, Q., Yan, G., Li, Z-L., et al. (2015). Atmospheric water vapor retrieval from Landsat 8 thermal infrared images. *Journal of Geophysical Research-Atmospheres*, 120, 1723–1738.
- Santamouris, M., Cartalis, C., Synnefa, A., & Kolokotsa, D. (2015). On the impact of urban heat island and global warming on the power demand and electricity consumption of buildings-A review. *Energy and Buildings*, 98, 119–124.
- Sobstyl, JM., Emig, T., Qomi, MJA., Ulm, FJ., & Pellenq, RJM. (2018). Role of City Texture in Urban Heat Islands at Nighttime. *Physical Review Letters*, 120.
- Stewart, ID., & Oke, TR. (2012). L CLIMATE ZONES FOR URBAN TEMPERATURE STUDIES. *Bulletin of the American Meteorological Society*, 93, 1879–1900.
- Streutker, DR. (2002). A remote sensing study of the urban heat island of Houston, Texas. *International Journal of Remote Sensing*, 23, 2595–2608.
- Sun, F., Liu, M., Wang, Y., Wang, H., & Che, Y. (2020). The effects of 3D architectural patterns on the urban surface temperature at a neighborhood scale: Relative contributions and marginal effects. *Journal of Cleaner Production*, 258.
- Sun, F., Zhao, H., Deng, L., Liu, Y., Cheng, R., & Che, Y. (2021). Characterizing the warming effect of increasing temperatures on land surface: Temperature change, heat pattern dynamics and thermal sensitivity. *Sustainable Cities and Society*, 70.
- Tian, Y., Zhou, W., Qian, Y., Zheng, Z., & Yan, J. (2019). The effect of urban 2D and 3D morphology on air temperature in residential neighborhoods. *Landscape Ecology*, 34, 1161–1178.
- Wan, KKW., Li, DHW., Pan, W., & Lam, JC. (2012). Impact of climate change on building energy use in different climate zones and mitigation and adaptation implications. *Applied Energy*, 97, 274–282.
- Wu, Z., Yao, L., Zhuang, M., & Ren, Y. (2020). Detecting factors controlling spatial patterns in urban land surface temperatures: A case study of Beijing. *Sustainable Cities and Society*, 63.
- Yan, H., Wang, K., Lin, T., Zhang, GQ., Sun, CG., Hu, XY., et al. (2021). The Challenge of the Urban Compact Form: Three-Dimensional Index Construction and Urban Land Surface Temperature Impacts. *Remote Sensing*, 13, 23.
- Yang, J., Wang, Y., Xiao, X., Jin, C., Xia, J., & Li, X. (2019). Spatial differentiation of urban wind and thermal environment in different grid sizes. *Urban Climate*, 28.
- Yu, SY., Chen, ZQ., Yu, BL., Wang, L., Wu, B., Wu, JP., et al. (2020a). Exploring the relationship between 2D/3D landscape pattern and land surface temperature based on explainable eXtreme Gradient Boosting tree: A case study of Shanghai, China. *Science of the Total Environment*, 725, 15.
- Yu, Z., Chen, S., Wong, NH., Ignatius, M., Deng, J., He, Y., et al. (2020b). Dependence between urban morphology and outdoor air temperature: A tropical campus study using random forests algorithm. *Sustainable Cities and Society*, 61.
- Zhao, L., Lee, X., Smith, RB., & Oleson, K. (2014). Strong contributions of local background climate to urban heat islands. *Nature*, 511, 216–219.
- Zheng, Z., Zhou, W., Wang, J., Hu, X., & Qian, Y. (2017). Sixty-Year Changes in Residential Landscapes in Beijing: A Perspective from Both the Horizontal (2D) and Vertical (3D) Dimensions. *Remote Sensing*, 9.
- Zheng, Z., Zhou, W., Yan, J., Qian, Y., Wang, J., & Li, W. (2019). The higher, the cooler? Effects of building height on land surface temperatures in residential areas of Beijing. *Physics and Chemistry of the Earth*, 110, 149–156.
- Zhou, D., Xiao, J., Bonafoni, S., Berger, C., Deilami, K., Zhou, Y., et al. (2019). Satellite Remote Sensing of Surface Urban Heat Islands: Progress, Challenges, and Perspectives. *Remote Sensing*, 11.